Chapter 5

Novel TiO_2 Photocatalyst Using Nonaqueous Solvent-Controlled Sol-Gel Route

Inderjeet Singh and Balaji I. Birajdar

Additional information is available at the end of the chapter

http://dx.doi.org/10.5772/intechopen.74568

Abstract

Synthesis of metal oxide nanoparticles with tailored properties is of great interest because of their potential in environmental, sensor, biomedical and energy applications. Specifically, TiO_2 gets special attention because of its high stability, biocompatibility, tunable band gap and surface properties. Aqueous sol-gel routes for the synthesis of TiO_2 nanoparticles are well established but suffer from little control over morphology and reproducibility. Nonaqueous solvent controlled sol-gel routes are good alternative to aqueous routes for the synthesis of highly crystalline TiO_2 nanoparticles with high purity and controlled doping of large size metallic ions. Present chapter describes the successful doping of large sized Zr and Na metal ions at Ti site and their influence on photo catalytic activity of TiO_2. The higher photo catalytic activity (even better than commercially available Degussa P25) of metal doped TiO_2 nanopowder is attributed to large surface area and reduced electron-hole recombination rate.

Keywords: TiO_2, metal-doped TiO_2, nanoparticle, nonaqueous, solvent controlled, sol-gel, photocatalytic activity

1. Introduction

Metal oxide nanoparticles (MONPs) are well-known for their outstanding role especially for environmental, sensor, biomedical and energy applications [1–10]. Among MONPs, TiO_2 nanoparticles are least toxic [11] and therefore synthesis of nanostructured TiO_2 with tailored properties has been most extensively investigated in recent years.TiO_2 occurs in three different phases [12], anatase, rutile and brookite with rutile as most stable phase and anatase as most desirable phase. TiO_2 is associated with outstanding properties including high stability,

exceptional biocompatibility, corrosion resistance, high photosensitivity and reactivity, as well as cost-effective and easy synthesis [13–16]. Semiconducting nature of anatase TiO_2 (Band gap of 3.2 eV) [17] allows it to degrade toxic organic compounds into simple hydrocarbons such as CO_2 and H_2O under UV irradiation. Under UV irradiation of energy greater than or equal to energy gap of TiO_2, electrons and holes are produced in valence band and conduction band, respectively. These electrons and holes result in formation of oxygen active species (OH*, H_2O_2, O_2^-, $^1O_2$) at surface of TiO_2, which reacts with toxic organic compounds and decompose them. Thus, TiO_2 is well known photocatalyst largely utilized for water reclamation, air purification, soil remediation, surface wettability adjustment, bacteria killing, solar cells, sensors, self-cleaning and anti-reflective surfaces [18–25].

A large number of synthesis methods have been employed for designing of TiO_2 nanoparticles with controlled shape, size, good yield and high dispersibility (less agglomeration). The shape and size of nanoparticles greatly affect the photocatalytic performance of the photocatalyst [26, 27]. Highly pure metal oxides can be prepared by conventional solid state route [28], but high processing temperature requirement limits its frequent use for synthesis. The biological synthesis method [11, 29] leads to formation of cost-effective, mono-dispersed nanoparticles but reproducibility needs improvement. To overcome all these difficulties during nanoparticles synthesis, alternative well-known liquid phase synthesis methods such as sol-gel [30, 31], hydrothermal [32, 33], microemulsion [34, 35], reverse microemulsion [36], sonochemical [37, 38] and microwave [39, 40] are employed. Among these synthesis methods, the sol-gel synthesis route gets special attention because of following reasons:

1. Homogeneity of starting precursor at molecular scale.
2. Low processing temperature.
3. Cost-effective.
4. Easy doping.

Sol-gel route can also yield multifold nanostructures such as nanoparticle, nanorods, nanotubes, aerogels and zeolites at a single platform. In addition, good yield and reproducibility are the key features of sol-gel route.

The present chapter will highlight the features of nonaqueous solvent controlled sol-gel route for the synthesis of pure and metal doped TiO_2 nanoparticles. Effects of metal doping and synthesis strategy on structural and surface properties are correlated with photocatalytic activity of pure and metal doped TiO_2 photocatalyst.

2. Synthesis

2.1. General overview

The sol-gel route [41, 42] involves the mixing of metal precursor into either water or organic solvent followed by formation of 3-dimensional network resulting in viscous gel, which in

http://dx.doi.org/10.5772/intechopen.74568

general results in amorphous powder after drying process. The process of mixing is known as hydrolysis, while formation of 3-dimensional network is called as condensation. These two processes are further controlled by many parameters including nature of metal precursor, ratio of precursor to solvent, nature of solvent, capping agents (surfactants), pH and temperature. **Figure 1** summarizes the various types of sol-gel routes.

Aqueous sol-gel route [41], as its name suggests, uses water as solvent to dissolve metal precursor and to complete hydrolysis process. The hydrolysis process is extremely fast due to high reactivity of water with precursors and therefore, generally there is little control over morphology and reproducibility. Nonaqueous sol-gel routes offer a good alternative to get rid of these difficulties [43, 44]. An organic solvent (alcohols, ketones, aldehydes or ethers) is used to complete the hydrolysis process instead of water. Besides, the oxygen required for metal-oxide formation is supplied by organic solvent in nonaqueous sol-gel route, whereas water plays the role of oxygen donor in aqueous sol-gel synthesis. However, inclusion or exclusion of some surfactant (consisting of hydrophilic and hydrophobic groups) in reaction solution further classifies the nonaqueous sol-gel route into surfactant assisted and solvent controlled (surfactant free) routes respectively. The main advantage of surfactant assisted nonaqueous sol-gel route is that the surfactant acts as capping agent and results in highly mono-dispersed nanoparticles. In addition a good control over particle size, morphology with outstanding reproducibility is direct consequence of surfactant-assisted nonaqueous sol-gel route. Moreover, the surface properties of nanoparticles can be easily tailored by exchanging surfactants with other functional groups. However this method is also prone to certain limitations like impurities in nanoparticles and toxic effects due to surfactants. These limitations impose restrictions on the surface sensitive applications (photocatalytic, biomedical and sensing) of nanoparticles.

2.2. Solvent controlled nonaqueous sol-gel route

A good alternative to surfactant assisted nonaqueous sol-gel route [45, 46] is solvent controlled nonaqueous sol-gel route. The solvent in itself plays role of oxygen donor necessary for oxide formation and stabilizing agent to control shape, size and morphology of nanoparticles. This modified sol-gel route also facilitates highly pure nanoparticles completely free

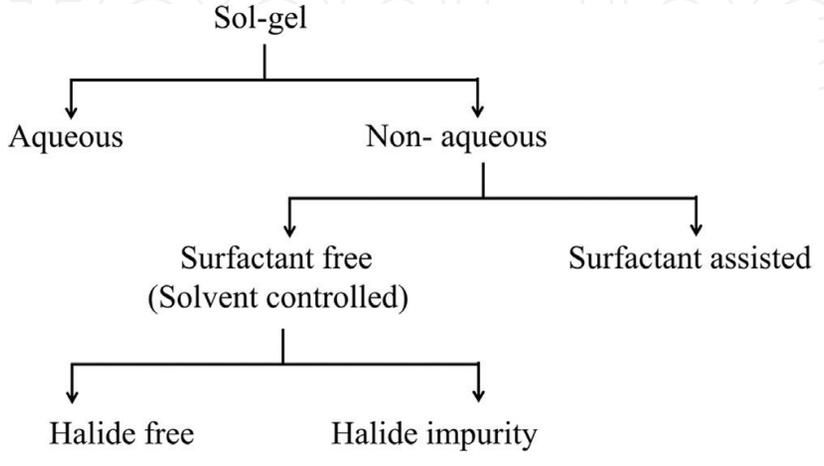

Figure 1. Various types of sol–gel synthesis routes.

from toxic surfactants but suffers from tendency to agglomerate. However toxic effect of halides cannot be neglected when metal oxide nanoparticles are prepared by reacting metal halides with organic solvents. In order to avoid halide impurities from metal oxide nanoparticles it is wise to use metal alkoxides, acetates or acetylacetonates as metal precursor. In the following subsections, synthesis of pristine and metal doped TiO_2 nanoparticles using halide free, nonaqueous, solvent controlled sol-gel route [2, 10] is described.

2.2.1. Synthesis of pristine TiO_2

Titanium tetra iso-propoxide (TTIP) was used as Titanium precursor and methoxyethanol as organic solvent. 20 ml TTIP is added to 40 ml methoxyethanol and mixed using magnetic stirrer. The pH of solution is adjusted to value 3 using 1 M HNO_3, which also catalyzes the hydrolysis process. The mixing is continued until viscous gel is formed, which is then dried under IR lamp and pulverized to obtain amorphous powder. The pure anatase TiO_2 nanopowder is formed after calcining the amorphous powder at 450°C for 1 hour. The chemical reactions occurring during hydrolysis and condensation in the synthesis are listed below.

$$\mathrm{Ti\,[OR]_4 + 4\,HOR' \rightarrow Ti\,[OH]_4 + ROR'\ (Hydrolysis)}$$

$$\mathrm{Ti\,[OH]_4 \rightarrow TiO_2 + 2\,H_2O\ (Condensation)}$$

2.2.2. Synthesis of metal doped TiO_2

What is the motivation for metal doping in TiO_2? As explained earlier, TiO_2 is wide band gap semiconductor and requires UV irradiation for its operation as a photo catalyst. The contribution of UV light in the solar radiation is less than 5%. Therefore, it is required to tune the band gap of TiO_2 to visible range so that no extra source of radiation energy (other than solar light) is required. Also, pristine TiO_2 suffers from higher recombination rate of charge carriers (electron and hole) resulting in less photocatalytic efficiency. Metals [10, 47–52] and nonmetals [53–58] are well known for their ability to reduce the band gap of TiO_2 by generating energy states between valence band and conduction band. These energy states serve as charge carrier trapping center and therefore reduce the electron hole recombination rate. The reduction in electron hole recombination rate results in remarkable improvement in photocatalytic performance. In addition, noble metals (Ag, Au and Pt), transition metals [59–61] and nonmetals doping in TiO_2 reduces the band gap of TiO_2 to visible range. Moreover, many doped TiO_2 nanoparticles are found to have small size as compared to pristine TiO_2, which improves the surface area and consequently boosts up the photocatalytic performance. However, favorable change in properties of TiO_2 by doping is largely affected by synthesis methods.

In current chapter, synthesis and photocatalytic properties of TiO_2 nanoparticles doped with one transition metal, Zirconium (Zr) and one other alkali metal, sodium (Na) are discussed. Both these metals have higher ionic radii (~0.79 Å for Zr and ~1.02 Å for Na) as compared to titanium (~0.68 Å for Ti). Large ionic radii and low valence ionic metallic dopant in host Ti4+ always results in strain in the crystal structure that favors the formation of oxygen vacancies [62]. These oxygen vacancies are prone to trap electrons and suppress grain growth resulting

in reduced charge recombination rate and small crystallite size respectively. There are many reports which claimed contradictory reports on photocatalytic activity of TiO_2 after doping of same dopant under different synthesis routes. Bessekhouad et al. [63] compared the photo catalytic efficiency of Na doped TiO_2 nanopowder prepared via two methods: sol-gel route and impregnation technology. They found that photo catalytic efficiency of nanopowder prepared by impregnation technology is higher than nanopowder prepared by aqueous sol-gel route. In addition, Na doping in TiO_2 matrix via aqueous sol-gel route decreases the photocatalytic efficiency due to migration of Na at TiO_2 surface instead of entering in the lattice. On the other hand, Yang et al. [64] showed higher photocatalytic activity of Na doped TiO_2 nanopowder prepared via solvothermal method. XRD analysis by Yang et al. [64], Xie et al. [65] as well as Bessekhouad et al. [63] could not confirm the doping of large sized Na into TiO_2 lattice and therefore hinted at the tendency of large sized Na + ions to migrate to TiO_2 surface. Therefore, it is required to study the effect of synthesis method on doping mechanism and photocatalytic activity of large sized metal dopants in TiO_2 matrix.

In [2, 10] Zr and Na has been doped in TiO_2 matrix individually by solvent controlled nonaqueous sol-gel route. Easily dissolvable zirconium oxy-nitrate and sodium nitrate are used as precursor of Zr and Na respectively. To achieve nominal dopants concentration, calculated amount of precursor is added to solvent prior to addition of Ti precursor. After complete dissolution of dopant precursor, Ti precursor is added to reaction solution and similar steps are followed as in preparation of doped TiO_2 nanopowder.

3. Characterization of pristine and metal doped TiO_2

3.1. Phase and structural characterization

X-ray diffraction (XRD) is an important tool used to determine the phase purity of sample, crystal structure, lattice parameter, average crystallite size and quantitative phase analysis. Generally, as prepared TiO_2 by sol-gel route is amorphous and therefore requires different heat treatment to form crystalline phases. Low (300–500°C), moderate (500–700°C) and high (more than 700°C) calcination temperature results in pure anatase phase, mixture of anatase and rutile, and pure rutile phase respectively [66]. The anatase to rutile (A-R) phase transformation is largely affected by type and amount of metal doping. Choi et al. [67] studied effect of single metal ion doping on A-R phase transformation temperature in TiO_2 prepared by sol-gel route. They observed that many metals such as Pt, Cr, V, Fe, La doping in TiO_2 lowers the A-R transformation temperature, whereas Ru metal shows opposite behavior. Xie et al. [65] and Singh et al. [2] also reported increased A-R transformation temperature in Na doped TiO_2 nanopowder. The presence of rutile structure in anatase phase affects the photocatalytic activity of metal doped TiO_2.

Figure 2(A) and **Figure 2(B)** shows the XRD pattern of Zr doped TiO_2 and Na doped TiO_2 with pristine TiO_2 respectively. Very fine powders of TiO_2 based photocatalysts prepared by nonaqueous solvent controlled sol-gel route [2, 10] are used to perform XRD using Cu Kα radiation (0.154 nm). Clearly, pure anatase phase of TiO_2 is formed for pristine as well as in Zr and Na doped TiO_2 nanopowder and matches with JCPDS card number 841286. In general, there are two types of doping (i) substitutional, and (ii) interstitial. Which one of these two

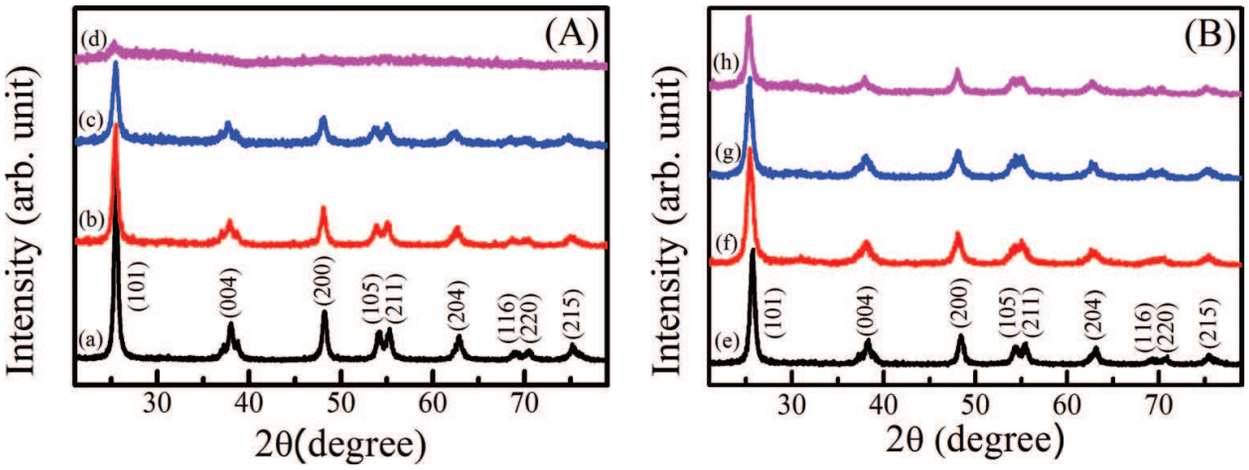

Figure 2. The XRD patterns of Zr (A) and Na (B) doped TiO_2 nano-powder calcined at 450°C for 1 hr.: (a & e) pristine TiO_2; (b) $Ti_{0.95}Zr_{0.05}O_2$; (c) $Ti_{0.90}Zr_{0.10}O_2$; (d) $Ti_{0.85}Zr_{0.15}O_2$; (f) $Ti_{0.96}Na_{0.04}O_2$; (g) $Ti_{0.92}Na_{0.08}O_2$ and (h) $Ti_{0.90}Na_{0.10}O_2$. Figure (A) reprinted with permission from Reference [10]. Copyright 2017, Elsevier.

types of doping is favored, depends on size of guest ion as compared to host ion and volume size of interstitial position in the host lattice. Substitutional doping is preferred in case where size of guest ion is comparable or slightly larger than lattice ion, whereas if size of guest ion is much smaller than lattice ion then it occupies interstitial position of host lattice.

XRD peaks of crystal planes of Zr doped TiO_2 (**Figure 2(A)**) shows red shift in 2θ values, which confirms the substitutional doping of Zr^{4+} at Ti^{4+} site [10]. The substitutional doping of Zr in TiO_2 results in an increase in cell parameter and cell volume as reported by Yu et al. [68] and Wang et al. [69] Thus, incorporation of large sized Zr results in lattice strain and hence leads to formation of oxygen vacancies and suppresses the grain growth. Similar behavior is observed for Na doped TiO_2 nanopowder (**Figure 2(B)**) [2]. However formation of oxygen vacancies in Na doped TiO_2 can occur not only due to strain induced by Na doping but also due to lower valence state of Na^{+1} ion. It should be noted that there are contradictory literature reports regarding doping of Na in TiO_2. Xie et al. [65] who used aqueous sol-gel synthesis, reported that large size Na cannot substitute Ti and therefore migrates to TiO_2 surface forming Na-O bonds as there is no peak shift is observed in XRD patterns. Thus it appears that substitutional doping of Na at Ti in TiO_2, as indicated by the XRD peak shifts in **Figure 2(B)**, is facilitated by nonaqueous solvent controlled sol-gel route, which was used by Singh et al. [10].

The crystallite size of pristine and doped TiO_2 nanopowder are calculated by well-known Debye Scherrer formula and tabulated in **Table 1**. In both, Zr doped TiO_2 and Na doped TiO_2, the crystallite size reduces for certain dopant concentration and hence increases the surface area of nanoparticles. Additionally, A-R phase transformation temperature is increased due to doping Zr^{4+} and Na^{+1} in TiO_2 matrix [10, 65, 68, 69].

3.2. Microstructural characterization

XRD gives structural information like lattice constant and crystalline phases averaged over bulk of the material. TEM on the other hand is able to give microstructural information on

http://dx.doi.org/10.5772/intechopen.74568

Sample	TiO_2	$Ti_{0.95}Zr_{0.05}O_2$	$Ti_{0.9}Zr_{0.1}O_2$	$Ti_{0.96}Na_{0.04}O_2$	$Ti_{0.92}Na_{0.08}O_2$	$Ti_{0.9}Na_{0.1}O_2$
Particle size (nm)	19.0	14.0	11.0	11.0	10.5	11.0

Table 1. Particle size (calculated by Debye Scherrer formula) of pristine and metal doped TiO_2 nanoparticles.

a nano meter length scale. In addition, grain boundaries, dislocations and structural defects could be easily identified by TEM. In this technique, a well-focused electron beam impinges on an ultrathin specimen in a high vacuum column, with the help of electromagnetic lenses. The impinged electron beam interacts with specimen and gets transmitted. A controlled and sophisticated system of electromagnetic lenses is used to focus the transmitted electron beam on a fluorescent screen. Selected area electron diffraction, diffraction contrast imaging, high resolution imaging and energy dispersive X-ray spectroscopy are some of the most commonly used TEM techniques for the characterization of materials.

Figure 3 shows the bright field TEM images, selective area electron diffraction (SAED) patterns and HRTEM images of pristine and metal doped TiO_2 nanopowder prepared by nonaqueous solvent controlled sol-gel route. Clearly, the particle size reduces with metal doping in comparison to pristine TiO_2, which is in agreement with XRD results. The SAED ring pattern and HRTEM images confirm the crystalline nature of pristine as well as metal doped TiO_2 nanoparticles. The SAED diffraction rings could be indexed as (101), (004) and (200) lattice planes of pristine anatase TiO_2. The increase in lattice spacing with Zr and Na doping indicates large metal ion substitution at Ti site in agreement with XRD results.

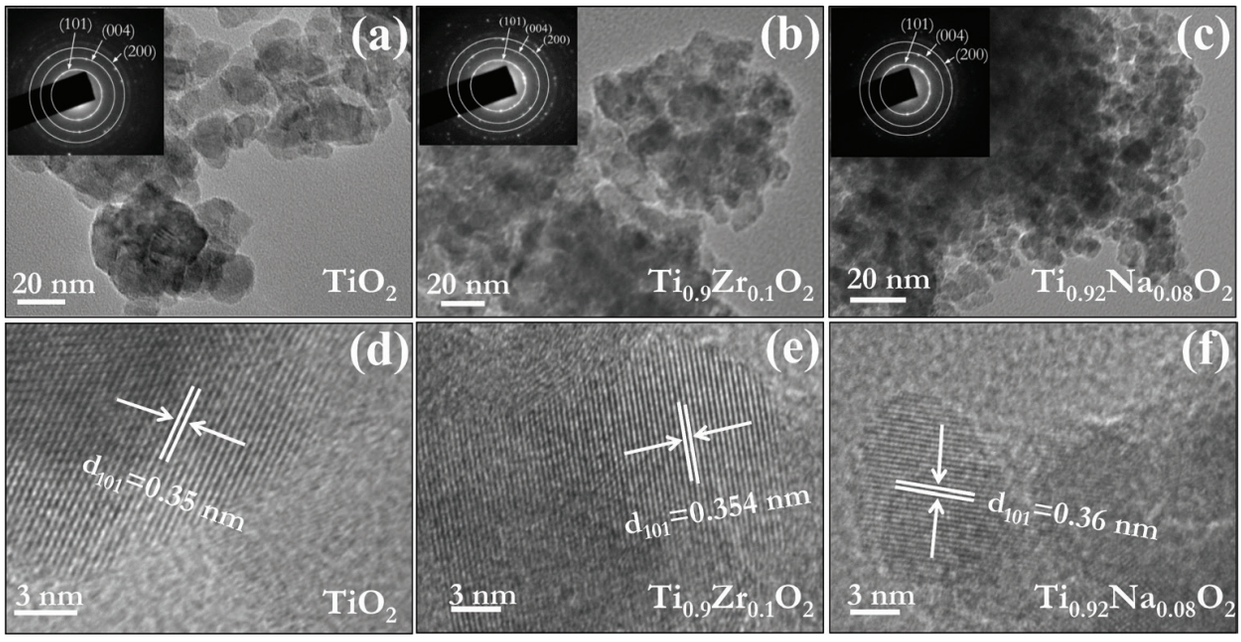

Figure 3. TEM images (a, b and c with insets shows respective selective area electron diffraction pattern) and HRTEM images (d, e and f). Figure (b&e) reprinted with permission from Ref. [10]. Copyright 2017, Elsevier.

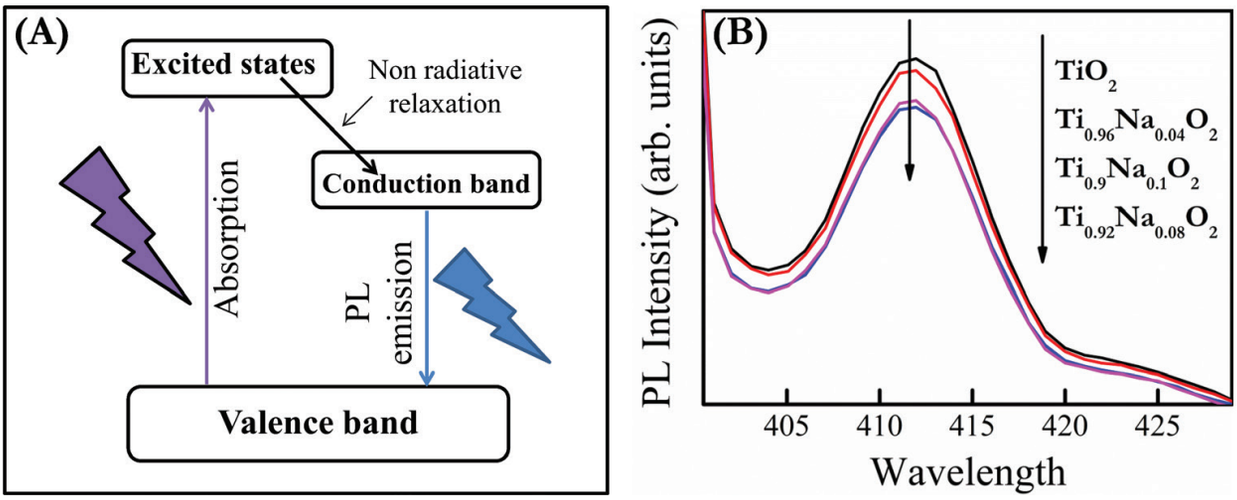

Figure 4. (A) Principle of photoluminescence spectroscopy. (B) PL spectra of pristine and Na doped TiO_2 nanopowder.

3.3. Photoluminescence study

Photoluminescence (PL) spectroscopy is a versatile and powerful optical method to investigate the energy levels in materials. The material is irradiated with light photons of energy greater than or equal to band gap energy of material. This results in the excitation of electrons from valence band to the excited states (**Figure 4(A)**) of material. These electrons relax to conduction band by losing excess energy via nonradiative process. When these electrons return to their valence band, the energy is released in the form of photons and the process is known as photoluminescence. The energy of emitted photons is determined by the difference in atomic energy levels, while the intensity of emitted light gives us information regarding recombination of electrons and holes.

The energy and intensity of emitted light in PL spectra of particular material is highly affected by doping. **Figure 4(B)** shows the PL spectra of pristine and Na doped TiO_2 nanopowder at excitation wavelength 390 nm. The shape of PL signal remains same while intensity reduces with increase in doping concentration of Na in TiO_2 matrix. This is attributed to the fact that Na doping in TiO_2 matrix results in formation of oxygen vacancies resulting in energy states lying between valence band and conduction band that trap the electrons form conduction band and thereby reduce electron-hole recombination [68]. However, the PL signal intensity increases for $Ti_{0.9}Na_{0.1}O_2$ sample. This is attributed to fact that excessive formation of oxygen vacancies might act as recombination centers [70].

4. Photocatalytic activity

The photocatalytic activity of prepared photo catalyst can be measured by many different test methods [71], which have been accepted at national and international standards. We have used German standard DIN 52980[11] for the determination of photocatalytic activity. This standard

http://dx.doi.org/10.5772/intechopen.74568

method is based on the degradation of organic dye methylene blue (MB) by photo catalyst under UV irradiation. The degradation results are further confirmed by measuring total organic carbon (TOC) of initial dye aqueous solution and degraded dye aqueous solution by TOC analyzer.

4.1. Degradation experiment

The photocatalytic activity of pristine and metal doped TiO_2 is evaluated by degrading aqueous solution of MB dye under ultraviolet (UV) irradiation. In order to compare photocatalytic activity of photo catalyst prepared by nonaqueous solvent controlled sol-gel route with commercial photo catalyst, the photocatalytic activity of well-known commercially available Degussa P25 TiO_2 is also evaluated. The initial concentration of MB aqueous solution is 5 mg/L. About 100 ml of MB dye aqueous solution (pH 5) is taken in 100 ml borosil glass beaker and 60 mg of photo catalyst is added in the solution. The beaker is kept on magnetic stirrer for uniform suspension of photo catalyst in the solution throughout the experiment. The reaction mixture is irradiated by UV light of peak wavelength at 365 nm and the intensity of UV light at the surface of reaction mixture is 10 mW/cm^2. The distance between reaction mixture and UV light source is 20 cm resulting in light intensity of 8×10^4 lux over reaction mixture. In order to complete adsorption-desorption equilibrium between photo catalyst and dye, the reaction mixture is stirred for 20 minutes in completely dark chamber. After achieving adsorption-desorption equilibrium, the reaction mixture is irradiated with UV light and a small amount of solution is withdrawn at regular time intervals. The withdrawn sample is centrifuged to separate out nanoparticles from the solution and absorbance of supernatant measured using UV-Visible spectrometer. The photocatalytic degradation percentage of dye for different time intervals is plotted for several photo catalysts and without catalyst (WC).

The degradation percentage of dye is calculated using Eq. 1. The rate constant (k) for the photocatalytic degradation of dye is determined from pseudo first order law using Eq. 2.

$$\text{Degradation } \% = \left((C_0 - C_t)/C_0\right) \times 100 \tag{1}$$

$$\ln\left(C_0/C_t\right) = kt \tag{2}$$

where C_0 is dye concentration before UV irradiation and C_t is dye concentration after t time of UV irradiation.

In order to further confirm the degradation results, TOC of irradiated and nonirradiated dye aqueous solution is measured and TOC removal rate percentage is calculated using Eq. 3.

$$\text{TOC } \% = \left((TOC_0 - TOC_t)/TOC_0\right) \times 100 \tag{3}$$

where TOC_0 and TOC_t are the TOC values of dye solution before and after time 't' of UV irradiation respectively.

4.2. Degradation results and mechanism

The photocatalytic activity of prepared Na doped TiO_2 photo catalyst can be compared from **Figure 5**. Clearly, the degradation percentage of MB dye is highest for $Ti_{0.92}Na_{0.08}O_2$, even superior to commercially available Degussa P25 catalyst. The k values for degradation of MB dye by WC, P25, pristine TiO_2 and $Ti_{0.92}Na_{0.08}O_2$ are 0.86×10^{-3}, 30.52×10^{-3}, 3.02×10^{-3} and 43.24×10^{-3} min^{-1}, respectively. TOC results are in accordance as well. This enhancement in photocatalytic activity of TiO_2 with Na doping is attributed to its smaller crystallite size and reduced rate of electron-hole recombination. Similarly, $Ti_{0.9}Zr_{0.1}O_2$ shows enhanced photocatalytic activity [10] for which, in addition to reduction in crystallite size and electron-hole recombination, band gap was also reduced due to Zr doping.

The photocatalytic degradation of dye at the surface of TiO_2 is well explained in the existing literature [56, 72]. The reactions occurring at the surface of semiconductor TiO_2 under UV irradiation are depicted in the Eqs. 4–8. The electrons are excited to conduction band while holes are formed in conduction band after absorption of photons having energy greater than or equal to energy gap of semiconductor. In case of pristine TiO_2, most of these electrons recombine with holes; few of them react with adsorbed oxygen forming reactive oxygen active specie (ROS) O_2^-. Similarly holes in the valence band reacts with water molecules and form ROS OH* radicals. These ROS actually reacts with dye molecules and degrade them into simple hydrocarbons H_2O and CO_2.

$$TiO_2 + h\upsilon = e^- + h^+ \tag{4}$$

$$e^- + O_2 = O_2^- \tag{5}$$

$$H_2O + h^+ = OH^* + H^+ \tag{6}$$

$$O_2^- + 2H^+ + e^- = 2\,OH^* \tag{7}$$

$$MB + OH^* = \text{Degradation products} \tag{8}$$

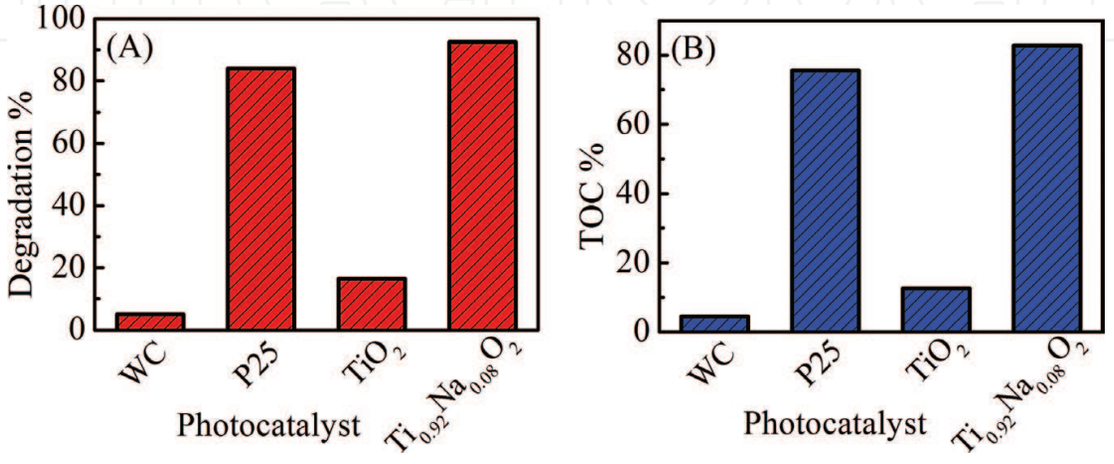

Figure 5. Photocatalytic degradation (A) and mineralization (B) of MB dye under 60 minute of UV irradiation.

http://dx.doi.org/10.5772/intechopen.74568

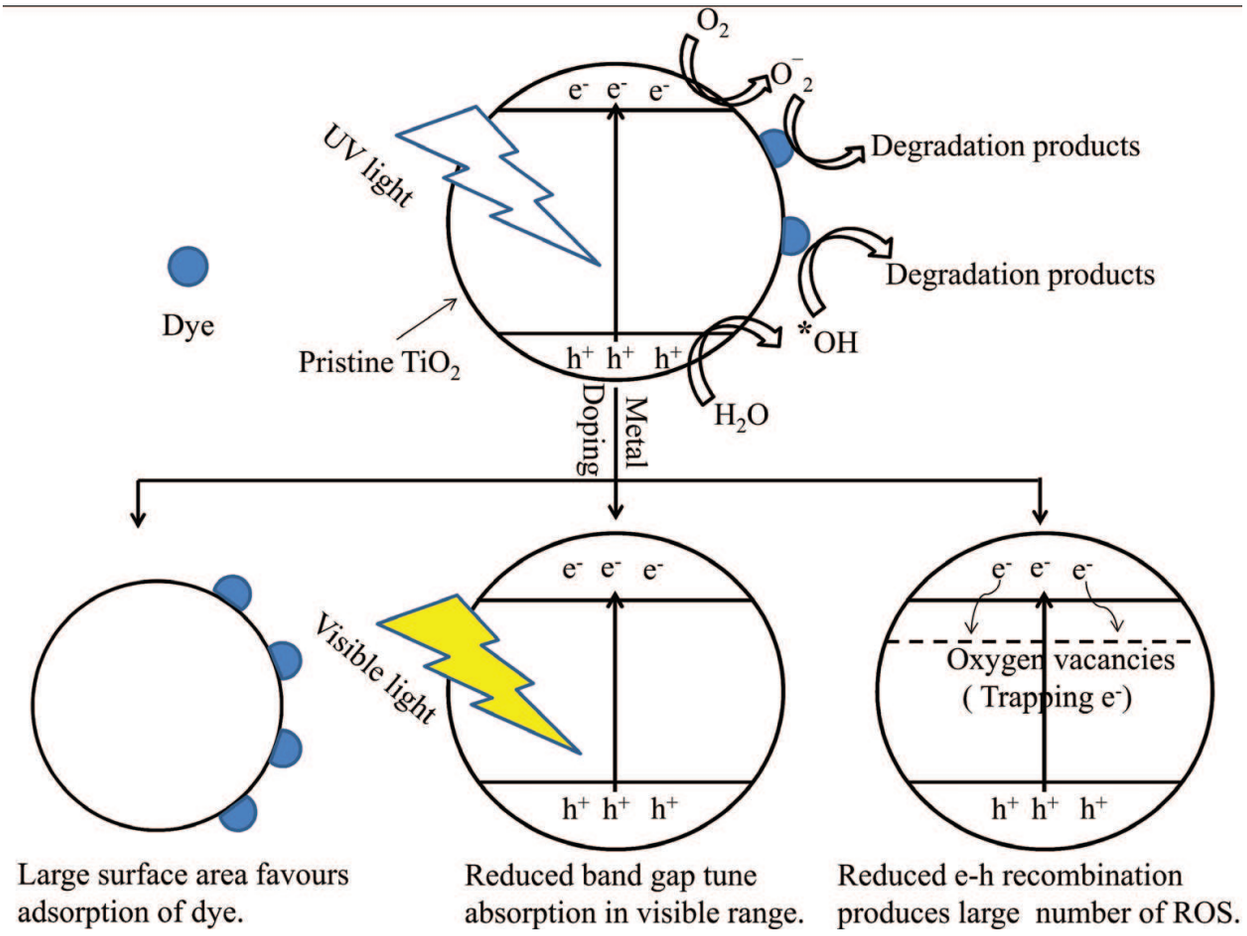

Figure 6. Effect of metal doping on degradation mechanism of pristine TiO_2.

In pristine TiO_2 the higher recombination rate of electron-hole results in fewer number of ROS radicals and hence less photocatalytic activity. In addition, large energy gap and small surface area also limit the degradation efficiency. Metal doping in TiO_2 results in large surface area, band gap tuning toward visible range and reduced electron-hole recombination rate. This most general proposed mechanism for degradation of dye at surface of metal doped TiO_2 is depicted in **Figure 6**.

5. Conclusion

In this chapter the importance of recently reported nonaqueous solvent controlled sol-gel route for the synthesis of metal doped TiO_2 with improved photocatalytic properties discussed. Pristine as well as Zr and Na doped TiO_2 nanoparticles have been prepared by this modified sol-gel route and their photocatalytic activity evaluated. Successful doping of these large metal ions in TiO_2 lattice using this synthesis route was confirmed by shifts in XRD peak positions and increase in d spacing observed from HRTEM images.

The photocatalytic activity of metal doped TiO_2 nanopowder is found to be much higher than pristine TiO_2, and even superior to commercially available Degussa P25 TiO_2 photo catalyst. This is attributed to large surface area due to small grain size and reduced electron hole

recombination due to formation of oxygen vacancies in metal doped TiO_2. The reduction in electron-hole recombination increases the availability of electrons and holes which reacts with adsorbed oxygen and water molecules forming large number of reactive oxygen active species leading to enhanced photocatalytic activity.

In past years, only few MONPs have been prepared by this nonaqueous, solvent controlled, sol-gel route. This method has great potential to synthesize functional nanoparticles of desired composition, size and surface properties essential for different applications.

Acknowledgements

We kindly acknowledge Jawaharlal Nehru University, New Delhi, India for financial support. I. Singh is thankful to university grant commission (UGC), India for providing SRF fellowship. B. Birajdar also acknowledges financial support via UPE-II (project ID 102) and DST purse-II.

Conflict of interest

There are no conflicts of interest to declare.

Author details

Inderjeet Singh and Balaji I. Birajdar*

*Address all correspondence to: birajdar@mail.jnu.ac.in

Special Centre for Nano Sciences, Jawaharlal Nehru University, New Delhi, India

References

[1] Tang SCN, Lo IMC. Magnetic nanoparticles: Essential factors for sustainable environmental applications. Water Research. 2013;**47**:2613-2632. DOI: 10.1016/j.watres.2013.02.039

[2] Singh I, Birajdar B. Synthesis, characterization and photocatalytic activity of mesoporous Na-doped TiO_2 nano-powder prepared via a solvent-controlled non-aqueous sol-gel route. RSC Advances. 2017;**7**:54053-54062. DOI: 10.1039/c7ra10108b

[3] Ngomsik AF, Bee A, Draye M, Cote G, Cabuil V. Magnetic nano- and microparticles for metal removal and environmental applications: A review. Comptes Rendus Chimie. 2005; **8**:963-970. DOI: 10.1016/j.crci.2005.01.001

[4] Karlsson HL, Cronholm P, Gustafsson J, Moeller L. Copper oxide nanoparticles are highly toxic: A comparison between metal oxide nanoparticles and carbon nanotubes. Chemical Research in Toxicology. 2008;**21**:1726-1732. DOI: 10.1021/tx800064j

[5] Rahman MM, Khan SB, Jamal A, Faisal M, Aisiri AM. Iron oxide nanoparticles. InTech Open; 2011. p. 43-66. DOI: 10.5772/27698

[6] Mir IA, Singh I, Birajdar B, Rawat K. A facile platform for photocatalytic reduction of methylene blue dye by CdSe-TiO_2 nanoparticles. Water Conservation Science and Engineering. 2017;**2**:43-50. DOI: 10.1007/s41101-017-0023-5

[7] Franke ME, Koplin TJ, Simon U. Metal and metal oxide nanoparticles in chemiresistors: Does the nanoscale matter? Small. 2006;**2**:36-50. DOI: 10.1002/smll.200500261

[8] Simon-Deckers A. Size-, composition- and shape-dependent toxicological impact of metal oxide nanoparticles and carbon nanotubes towards bacteria. Environmental Science and Technology. 2009;**43**:8423-8429. DOI: 10.1021/es9016975

[9] Sarkar S, Guibal E, Quignard F, SenGupta AK. Polymer-supported metals and metal oxide nanoparticles: Synthesis, characterization, and applications. Journal of Nanoparticle Research. 2012;**14**:1-24. DOI: 10.1007/s11051-011-0715-2

[10] Singh I, Kumar R, Birajdar BI. Zirconium doped TiO_2 nano-powder via halide free non-aqueous solvent controlled sol-gel route. Journal of Environmental Chemical Engineering. 2017;**5**:2955-2963. DOI: https://doi.org/10.1016/j.jece.2017.05.046

[11] Seabra A, Durán N. Nanotoxicology of metal oxide nanoparticles. Metals (Basel). 2015; **5**:934-975. DOI: 10.3390/met5020934

[12] Reyes-Coronado D, Rodr??guez-Gattorno G, Espinosa-Pesqueira ME, Cab C, De Coss R, Oskam G. Phase-pure TiO_2 nanoparticles: Anatase, brookite and rutile. Nanotechnology. 2008;**19**:145605-145614. DOI: 10.1088/0957-4484/19/14/145605

[13] Pillai SC, Periyat P, George R, McCormack DE, Seery MK, Hayden H, Colreavy J, Corr D, Hinder SJ. Synthesis of high-temperature stable anatase TiO_2 photocatalyst. Journal of Physical Chemistry C. 2007;**111**:1605-1611. DOI: 10.1021/jp065933h

[14] Karpagavalli R, Zhou A, Chellamuthu P, Nguyen K. Corrosion beheaviour and biocompatibility of nanostructured TiO_2 film on Ti6Al4V. Journal of Biomedical Materials Research Part A. 2007;**83**:97-103. DOI: 10.1002/jbm.a

[15] Tachikawa T, Fujitsuka M, Majima T. Mechanistic insight into the TiO_2 photocatalytic reactions: Design of new photocatalysts. Journal of Physical Chemistry C. 2007;**111**:5259-5275. DOI: 10.1021/jp069005u

[16] Zhu YF, Zhang L, Gao C, Cao LL. The synthesis of nanosized TiO$_2$ powder using a sol-gel method with TiCl$_4$ as a precursor. Journal of Materials Science. 2000;**35**:4049-4054. DOI: 10.1023/A:1004882120249

[17] Scanlon DO, Dunnill CW, Buckeridge J, Shevlin SA, Logsdail AJ, Woodley SM, Catlow CRA, Powell MJ, Palgrave RG, Parkin IP, Watson GW, Keal TW, Sherwood P, Walsh A, Sokol AA. Band alignment of rutile and anatase TiO_2. Nature Materials. 2013;**12**:798-801. DOI: 10.1038/nmat3697

[18] Ryu J, Choi W. Substrate-specific photocatalytic activities of TiO and multiactivity test for water treatment application substrate-specific photocatalytic activities of TiO 2 and

multiactivity test for water treatment application. Environmental Science & Technology. 2008;**42**:294-300. DOI: 10.1021/es071470x

[19] Obee TN, Brown RT. TiO_2 photocatalysis for indoor air applications: Effects of humidity and trace contaminant levels on the oxidation rates of formaldehyde, toluene, and 1,3-butadiene. Environmental Science & Technology. 1995;**29**:1223-1231. DOI: 10.1021/es00005a013

[20] Wang TC, Lu N, Li J, Wu Y. Plasma-TiO_2 catalytic method for high-efficiency remediation of p-nitrophenol contaminated soil in pulsed discharge. Environmental Science & Technology. 2011;**45**:9301-9307. DOI: 10.1021/es2014314

[21] Lai Y, Huang J, Cui Z, Ge M, Zhang KQ, Chen Z, Chi L. Recent advances in TiO_2-based nanostructured surfaces with controllable wettability and adhesion. Small. 2016;**12**:2203-2224. DOI: 10.1002/smll.201501837

[22] Wei C, Lin WY, Zainal Z, Williams NE, Zhu K, Kruzlc AP, Smith RL, Rajeshwar K. Bactericidal activity of TiO_2 photocatalyst in aqueous media: Toward a solar-assisted water disinfection system. Environmental Science & Technology. 1994;**28**:934-938. DOI: 10.1021/es00054a027

[23] Park N-G, van de Lagemaat J, Frank AJ. Comparison of dye-sensitized rutile- and anatase-based TiO_2 solar cells. The Journal of Physical Chemistry. B. 2000;**104**:8989-8994. DOI: 10.1021/jp994365l

[24] Kirner U, Schierbaum KD, Göpel W, Leibold B, Nicoloso N, Weppner W, Fischer D, Chu WF. Low and high temperature TiO_2 oxygen sensors. Sensors and Actuators B: Chemical. 1990;**1**:103-107. DOI: 10.1016/0925-4005(90)80181-X

[25] Zhang X, Fujishima A, Jin M, Emeline AV, Murakami T. Double-layered TiO_2-SiO_2 nanostructured films with self-cleaning and antireflective properties. The Journal of Physical Chemistry. B. 2006;**110**:25142-25148. DOI: 10.1021/jp064442u

[26] Wu N, Wang J, Tafen DN, Wang H, Zheng J-G, Lewis JP, Liu X, Leonard SS, Manivannan A. Shape-enhanced photocatalytic activity of single-crystalline anatase TiO_2 (101) nanobelts. Journal of the American Chemical Society. 2010;**132**:6679-6685. DOI: 10.1021/ja909456f

[27] Mclaren A, Valdes-Solis T, Li G, Tsang SC. Shape and size effects of ZnO nanocrystals on photocatalytic activity. Journal of the American Chemical Society. 2009;**131**:12540-12541

[28] Sun Z-P, Liu L, Zhang L, Jia D-Z. Rapid synthesis of ZnO nano-rods by one-step, room-temperature, solid-state reaction and their gas-sensing properties. Nanotechnology. 2006;**17**:2266-2270. DOI: 10.1088/0957-4484/17/9/032

[29] Durán N, Seabra AB. Metallic oxide nanoparticles: State of the art in biogenic syntheses and their mechanisms. Applied Microbiology and Biotechnology. 2012;**95**:275-288. DOI: 10.1007/s00253-012-4118-9

[30] Wang CC, Ying JY. Sol-gel synthesis and hydrothermal processing of anatase and rutile titania nanocrystals. Chemistry of Materials. 1999;**11**:3113-3120. DOI: 10.1021/cm990180f

[31] Niederberger M. Nonaqueous sol – gel routes to metal oxide nanoparticles. Accounts of Chemical Research. 2007;**40**:793-800. DOI: 10.1021/ar600035e

[32] Titirici MM, Antonietti M, Thomas A. A generalized synthesis of metal oxide hollow spheres using a hydrothermal approach. Chemistry of Materials. 2006;**18**:3808-3812. DOI: 10.1021/cm052768u

[33] Adschiri T, Hakuta Y, Sue K, Arai K. Hydrothermal synthesis of metal oxide nanoparticles at supercritical conditions. Journal of Nanoparticle Research. 2001;**3**:227-235. DOI: 10.1023/A:1017541705569

[34] Santra S, Tapec R, Theodoropoulou N, Dobson J, Hebard A, Tan W. Synthesis and characterization of silica-coated iron oxide nanoparticles in microemulsion: The effect of nonionic surfactants. Langmuir. 2001;**17**:2900-2906. DOI: 10.1021/la0008636

[35] Hingorani S, Pillai V, Kumar P, Multani MS, Shah DO. Microemulsion mediated synthesis of zinc-oxide nanoparticles for varistor studies. Materials Research Bulletin. 1993; **28**:1303-1310. DOI: 10.1016/0025-5408(93)90178-G

[36] Zarur A, Ying J. Reverse microemulsion synthesis of nanostructured complex oxides for catalytic combustion. Nature. 2000;**403**:65-67. DOI: 10.1038/47450

[37] Vijaya Kumar R, Diamant Y, Gedanken A. Sonochemical synthesis and characterization of nanometer-size transition metal oxides from metal acetates. Chemistry of Materials. 2000;**12**:2301-2305. DOI: 10.1021/cm000166z

[38] Guo J, Zhu S, Chen Z, Li Y, Yu Z, Liu Q, Li J, Feng C, Zhang D. Sonochemical synthesis of TiO_2 nanoparticles on graphene for use as photocatalyst. Ultrasonics Sonochemistry. 2011;**18**:1082-1090. DOI: 10.1016/j.ultsonch.2011.03.021

[39] Mirzaei A, Neri G. Microwave-assisted synthesis of metal oxide nanostructures for gas sensing application: A review. Sensors and Actuators B: Chemical. 2016;**237**:749-775. DOI: 10.1016/j.snb.2016.06.114

[40] Bilecka I, Djerdj I, Niederberger M. One-minute synthesis of crystalline binary and ternary metal oxide nanoparticles. Chemical Communications. 2008;**7**:886-888. DOI: 10.1039/B717334B

[41] Brinker CJ, Scherer GW. Sol-Gel_Science_The_physics_and_chemistry_of_sol-gel_processing_-_Brinker_1990.pdfl; 1990. 462. DOI:10.1016/S0254-0584(02)00315-2

[42] Kulkarni SK. Nanotechnology: Principles and Practices. 3rd ed. Chem: Springer; 2007. 103 p. DOI: 10.1007/978-3-642-227-6

[43] Niederberger M, Pinna N. Metal oxide nanoparticles in organic solvents: Synthesis formation, assembly and application. London: Springer; 2009. DOI: 10.1007/978-1-84882-671-7

[44] Niederberger M, Garnweitner G, Pinna N, Neri G. Non-aqueous routes to crystalline metal oxide nanoparticles: Formation mechanisms and applications. Progress in Solid State Chemistry. 2005;**33**:59-70. DOI: 10.1016/j.progsolidstchem.2005.11.032

[45] Niederberger M, Garnweitner G, Ba J, Polleux J, Pinna N. Nonaqueous synthesis, assembly and formation mechanisms of metal oxide nanocrystals. International Journal of Nanotechnology. 2007;**4**:263-281. DOI: 10.1504/IJNT.2007.013473

[46] Garnweitner G, Niederberger M. Nonaqueous and surfactant-free synthesis routes to metal oxide nanoparticles. Journal of the American Ceramic Society. 2006;**89**:1801-1808. DOI: 10.1111/j.1551-2916.2006.01005.x

[47] Wu P, Xie R, Imlay K, Shang JK. Visible-light-induced bactericidal activity of titanium dioxide codoped with nitrogen and silver. Environmental Science & Technology. 2010;**44**:6992-6997. DOI: 10.1021/es101343c

[48] Traversa E, Di Vona ML, Nunziante P, Licoccia S, Sasaki T, Koshizaki N. Sol-gel preparation and characterization of Ag-TiO_2 nanocomposite thin films. Journal of Sol-Gel Science and Technology. 2000;**19**:733-736. DOI: 10.1023/A:1008787412057

[49] Cao X, Liu C, Hu Y, Yang W, Chen J. Synthesis of N/Fe comodified TiO_2 loaded on bentonite for enhanced photocatalytic activity under UV-Vis light. Journal of Nanomaterials. 2016;**2016**:1-11. DOI: 10.115/2016/8182190

[50] Wu X, Yin S, Dong Q, Guo C, Kimura T, Matsushita J, Sato T. Photocatalytic properties of Nd and C codoped TiO_2 with the whole range of visible light absorption. Journal of Physical Chemistry C. 2013;**117**:8345-8352. DOI: 10.1021/jp402063n

[51] Zhang H, Chen G. potent antibacterial activities of Ag/TiO_2 nanocomposite powders synthesized by a one-pot sol-gel method. Environmental Science & Technology. 2009; **43**:2905-2910. DOI: 10.1021/es803450f

[52] Zhao G, Kozuka H, Yoko T. Sol-gel preparation and photoelectrochemical properties of TiO_2 films containing Au and Ag metal particles. Thin Solid Films. 1996;**277**:147-154. DOI: 10.1016/0040-6090(95)08006-6

[53] Eslami A, Amini MM, Yazdanbakhsh AR, Safari A, Asadi A. N, S co-doped TiO_2 nanoparticles and nanosheets in simulated solar light for photocatalytic degradation of non-steroidal anti-inflammatory drugs in water: A comparative study. Journal of Chemical Technology and Biotechnology. 2016;**91**:2693-2704. DOI: 10.1002/jctb.4877

[54] Liu JW, Han R, Wang HT, Zhao Y, Lu WJ, Wu HY, Yu TF, Zhang YX. Degradation of PCP-Na with La-B co-doped TiO_2 series synthesized by the sol-gel hydrothermal method under visible and solar light irradiation. Journal of Molecular Catalysis A: Chemical. 2011;**344**:145-152. DOI: 10.1016/j.molcata.2011.04.022

[55] Lu N, Quan X, Li J, Chen S, Yu H, Chen G. Fabrication of boron-doped TiO_2 nanotube array electrode and investigation of its photoelectrochemical capability. Journal of Physical Chemistry C. 2007;**111**:11836-11842. DOI: 10.1021/jp071359d

[56] Kumar SG, Devi LG. Review on modified TiO_2 photocatalysis under UV/visible light: Selected results and related mechanisms on interfacial charge carrier transfer dynamics. The Journal of Physical Chemistry. A. 2011;**115**:13211-13241. DOI: 10.1021/jp204364a

[57] Yu J, Zhou M, Cheng B, Zhao X. Preparation, characterization and photocatalytic activity of in situ N,S-codoped TiO_2 powders. Journal of Molecular Catalysis A: Chemical. 2006;**246**:176-184. DOI: 10.1016/j.molcata.2005.10.034

[58] Cho IS, Lee CH, Feng Y, Logar M, Rao PM, Cai L, Kim DR, Sinclair R, Zheng X. Codoping titanium dioxide nanowires with tungsten and carbon for enhanced photoelectrochemical performance. Nature Communications. 2013;**4**:1723. DOI: 10.1038/ncomms2729

[59] Obuya EA, Joshi PC, Gray TA, Keane TC, Jr WEJ. Application of Pt-TiO_2 nanofibers in photosensitized degradation of rhodamine B. International Journal of Chemistry. 2014;**6**:1-16. DOI: 10.5539/ijc.v6n1p1

[60] Haick H, Paz Y. Long-range effects of noble metals on the photocatalytic properties of titanium dioxide. The Journal of Physical Chemistry. B. 2003;**107**:2319-2326. DOI: 10.1021/jp026940i

[61] Epifani M, Giannini C, Tapfer L, Vasanelli L. Sol – gel synthesis and characterization of Ag and Au nanoparticles. Journal of the American Ceramic Society. 2000;**83**:2385-2393. DOI: 10.1111/j.1151-2916.2000.tb01566.x

[62] Pan X, Yang M-Q, Fu X, Zhang N, Xu Y-J. Defective TiO_2 with oxygen vacancies: Synthesis, properties and photocatalytic applications. Nanoscale. 2013;**5**:3601. DOI: 10.1039/c3nr00476g

[63] Bessekhouad Y, Robert D, Weber JV, Chaoui N. Effect of alkaline-doped TiO_2 on photocatalytic efficiency. Journal of Photochemistry and Photobiology A: Chemistry. 2004; **167**:49-57. DOI: 10.1016/j.jphotochem.2003.12.001

[64] Yang G, Yan Z, Xiao T, Yang B. Lowerature synthesis of alkalis doped TiO_2 photocatalysts and their photocatalytic performance for degradation of methyl orange. Journal of Alloys and Compounds. 2013;**580**:15-22. DOI: 10.1016/j.jallcom.2013.05.074

[65] Xie H, Li N, Liu B, Yang J, Zhao X. Role of sodium ion on TiO_2 photocatalyst: Influencing crystallographic properties or serving as the recombination center of charge carriers? Journal of Physical Chemistry C. 2016;**120**:10390-10399. DOI: 10.1021/acs.jpcc.6b01730

[66] Zhang J, Xu Q, Feng Z, Li M, Li C. Importance of the relationship between surface phases and photocatalytic activity of TiO_2. Angewandte Chemie, International Edition. 2008; **47**:1766-1769. DOI: 10.1002/anie.200704788

[67] Hoffmann MR. Effects of single metal-ion doping on the visible-light photoreactivity of TiO_2 effects of single metal-ion doping on the visible-light photoreactivity of TiO_2. Journal of Physical Chemistry C. 2010;**114**:783-792. DOI: 10.1021/jp908088x

[68] Yu JC, Lin J, Kwok RWM. Ti1-xZrxO2 solid solutions for the photocatalytic degradation of acetone in air. The Journal of Physical Chemistry. B. 1998;**102**:5094-5098. DOI: 10.1021/jp980332e

[69] Wang J, Yu Y, Li S, Guo L, Wang E, Cao Y. Doping behavior of Zr4+ ions in Zr4+−doped TiO_2 nanoparticles. Journal of Physical Chemistry C. 2013;**117**:27120-27126. DOI: 10.1021/jp407662d

[70] Bellardita M, Addamo M, Di Paola A, Palmisano L. Photocatalytic behaviour of metal-loaded TiO_2 aqueous dispersions and films. Chemical Physics. 2007;**339**:94-103. DOI: 10.1016/j.chemphys.2007.06.003

[71] Macías-Sánchez J, Hinojosa-Reyes L, Guzmán-Mar JL, Peralta-Hernández JM, Hernández-Ramírez A. Performance of the photo-Fenton process in the degradation of a model azo dye mixture. Photochemical & Photobiological Sciences. 2011;**10**:332-337. DOI: 10.1039/C0PP00158A

[72] Linsebigler AL, Linsebigler AL, Yates JT Jr, Lu G, Lu G, Yates JT. Photocatalysis on TiO_2 surfaces: Principles, mechanisms, and selected results. Chemical Reviews. 1995;**95**: 735-758. DOI: 10.1021/cr00035a013